ELSEVIER

The effect of selected parameters on ship collision results by dynamic FE simulations

Krzysztof Wiśniewski [*], Przemysław Kołakowski

Institute of Fundamental Technological Research (IFTR), Polish Academy of Sciences, ul. Świętokrzyska 21, 00-049 Warsaw, Poland

Abstract

The purpose of the paper is to study the effect of selected design parameters on crashworthiness of the struck ship. The dynamic collision process is simulated by the ABAQUS/Explicit code, and two problems are analysed: (1) a plate struck by a cone, and (2) a collision of two ships.

The first problem, of a plate struck by a rigid cone, has a preliminary character and validates our FE modelling; a similar crushing force is obtained as in Amdahl and Kavlie (DNV-MIT Workshop on Mechanics of Ship Collision and Grounding, DNV Høvik, Oslo, September) and Simonsen (ISESO Report No. I108.02.02.052.004, Department of Naval Architecture and Offshore Engineering, Technical University of Denmark, April), despite the differences in methods of analysis applied. The current computations go further than the cited papers, and assess the dependence of results on the material model of the plate (including failure), the contact within the plate interior, and the mass of the striking cone.

The second problem is of practical interest, as it concerns a collision of a double hull crude oil carrier ship and a container vessel with a bulbous bow. The progress of deformation in time is monitored including large plastic strains as well as contact between the ships, which allows to model crushing and tearing. The effect of the following parameters is assessed: the material model of the struck ship, the friction coefficient for the contact between the vessels, the initial velocity of the striking ship, the motion of the struck ship, and the mass scaling option used to accelerate computations.

The included results present the deformed struck objects, and also the crushing force and various types of energy vs. penetration of the striking body. Conclusions are formulated regarding the numerical method used, the striking ship velocity data and the material model for the struck ship. © 2002 Elsevier Science B.V. All rights reserved.

Keywords: Ship collision; Crashworthiness; FE simulations

---

[*] Corresponding author.

E-mail addresses: kwisn@ippt.gov.pl (K. Wiśniewski), pkolak@ippt.gov.pl (P. Kołakowski).

1. Introduction

Current guidelines of maritime classification societies are shifting from general regulations towards a more rational safety verification of individual ships, and hence it becomes important to establish a relationship between the features of the colliding ships and the resulting extent of damage, for various collision scenarios. This could be only feasible using efficient and sufficiently accurate tools of structural analysis, such as e.g. a dynamic FE code ABAQUS/Explicit applied in the present computations. Such codes not only allow to model the geometry and structural parts of colliding ships quite accurately, but are also able to deal with non-linear phenomena, such as crushing and tearing of the material, and to account for an in-time changing contact between ships.

As proposed by Minorsky [1], a collision problem is often split into the so-called external dynamics and the internal mechanics, where the first one is concerned with the global ships motions, while the second with the energy absorbed by the ships. The external dynamics typically involves several simplifications, see e.g. in Pedersen and Zhang [2], such as: (a) only dominant types of motion are considered, (b) the surrounding water is modelled by the added mass, and (c) the configuration of ships remains constant during the event. A more computer-oriented approach is presented in Lenselink and Thung [3], and the analysis is divided into three steps: (1) structure–structure collision calculations without the influence of the water, (2) water resistance calculations for a rigid motion of the struck ship, and (3) the combined fluid-structure calculations. It was found in this work that about 20% of the initial kinetic energy was dissipated by the water.

The present paper is concerned with the so-called internal mechanics of collision. Despite the earlier validation effort, e.g. of Wierzbicki [4], Lenselink and Thung [3], Wierzbicki [5], Sano et al. [6], Simonsen and Ocackli [7], it has been considered desirable to perform further comparisons using realistic ship collision scenarios (cf. Kitamura [11]). Two problems are analysed and a selection of key results is presented, partial results were presented in Wisniewski et al. [8].

First, a relatively simple example of a cone impacting on a plate of Amdahl and Kavlie [9] is analysed, in order to fully understand computational strategies available in the code, and to establish most efficient simulation strategy for subsequent simulation of ship collision. Similarity between the obtained results and the experimental and numerical results of Amdahl and Kavlie [9] and Simonsen [10] is demonstrated.

Next, a much more complicated problem of a collision of two ships, which is of our main interest, is undertaken. The analyses are tailored to assess the influence of the following features of the model on the double-hull ship response: (i) the material model, (ii) the friction coefficient for the contact between ships, (iii) the initial velocity of the striking ship, (iv) the motion of the struck ship, and (v) the mass scaling option used to accelerate computations.

The scope of the paper is as follows. In Section 2 a short characteristic of the dynamic algorithm used in ABAQUS/Explicit is given. In Section 3 the problem of an impact of a rigid cone on a plate is described; including the experiment arrangements, the FE model, numerical results, and a discussion of the model features. Section 4 presents the problem of two ships in collision; i.e. the geometry of the ships, the FE models and material data, numerical analyses and reference results, as well as comparisons for selected model parameters. The discussion of the obtained results is presented in Section 5.

2. Short characteristics of dynamic algorithm, software and computer

The non-linear dynamic analyses of our selected collision problems were performed by use of ABAQUS/Explicit code, Ver.5.8-14, and the algorithm implemented in this code is characterised below. The equation being solved is the dynamic equilibrium equation of the system,

$$\mathbf{M\ddot{u}}(t) + \mathbf{f}(t) - \mathbf{p}(t) = 0, \tag{1}$$

where $\mathbf{u}$ is a state vector (displacements or rotation parameters), $\mathbf{M}$ is the mass matrix, $\mathbf{f}$ is the internal force vector, $\mathbf{p}$ is the external load vector, and t denotes time. The time integration procedure implemented in the code is based on use of the lumped (diagonal) mass matrix and the explicit time integration scheme. The time step from t_n to t_{n+1} is performed as follows. First, the acceleration is computed from Eq. (1) written for time t_n, i.e.

$$\mathbf{\ddot{u}}_n = \mathbf{M}^{-1}[\mathbf{p}_n - \mathbf{f}(\mathbf{u}_n)], \tag{2}$$

where the mass matrix is lumped for greater efficiency. Then, the central difference operators,

$$\mathbf{\ddot{u}}_n = \frac{\mathbf{\dot{u}}_{n+1/2} - \mathbf{\dot{u}}_{n-1/2}}{1/2(\Delta t_n + \Delta t_{n+1})}, \tag{3}$$

$$\mathbf{\dot{u}}_{n+1/2} = \frac{\mathbf{u}_{n+1} - \mathbf{u}_n}{\Delta t_{n+1}}, \tag{4}$$

are used to compute the velocity $\mathbf{\dot{u}}_{n+1/2}$ from Eq. (3), and the displacement $\mathbf{u}_{n+1}$ from Eq. (4). We can see that the solution process was advanced in time using values known from the previous time step, i.e. the velocity $\mathbf{\dot{u}}_{n-1/2}$ and the displacement $\mathbf{u}_n$. This scheme is only conditionally stable, and hence the size of the time increment is limited; for details on the control of the step size in the code see the ABAQUS/Explicit User's Manual.

This explicit solution strategy is very efficient because the stiffness matrix does not need to be formulated and factorised, and no iterations are performed. It is well suited to define general contact conditions and accommodate large rotations and large strains, which allows to model crushing and tearing.

The computations were performed on the Sun HPC Enterprise 10 000 (Starfire) computer of 12 processors 400 MHz, architecture SMP, RAM 2048 MB, OS Solaris 7, HPC. The computing power: $R_{\max} = 8.25$ Gflops, $R_{\text{peak}} = 9.6$ Gflops.

3. Indentation of plate by rigid cone

3.1. Experiment description

Experimental tests, described in Amdahl and Kavlie [9], were performed to study the behaviour of a double-hull plate under a deep indentation by a rigid cone. The experimental stand is shown in Fig. 1.

The arrangement of the plate, which was used in the test selected for comparison, is shown in Fig. 2. Note that the cone is pushed at the centre of the plate, between two longitudinal girders (marked with dashed vertical lines in the plan), right onto the transverse stiffening frame.
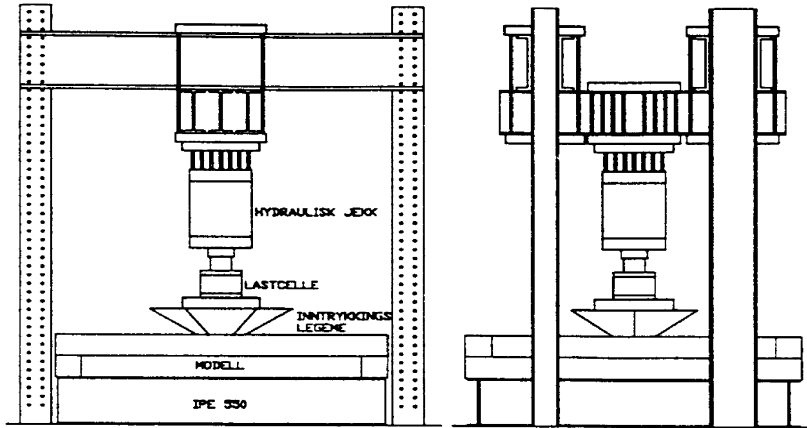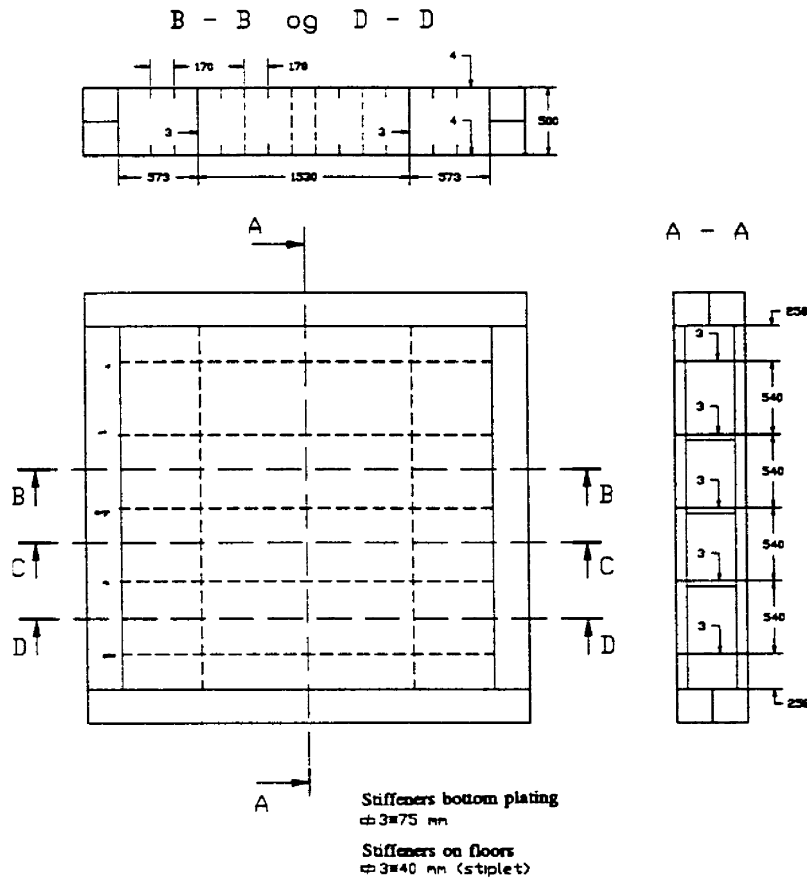
Fig. 1. Experimental stand of Amdahl and Kavlie [9].

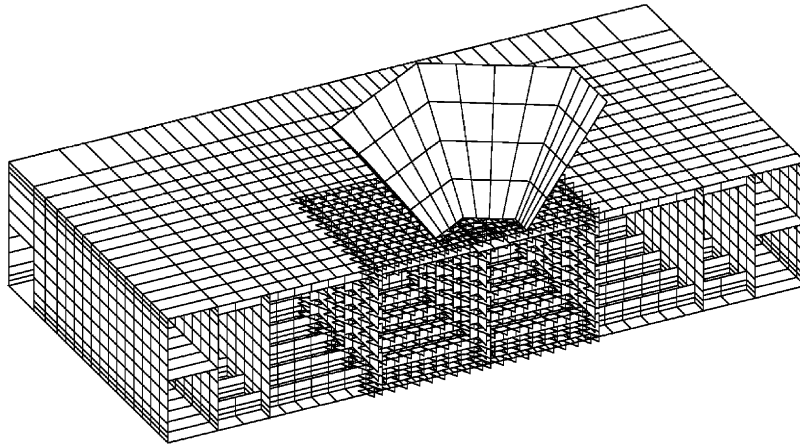Fig. 2. Plate in Test 2 by Amdahl and Kavlie [9].

Fig. 3. Finite element model of the plate and the impacting cone.

3.2. Finite element models and input data

Dimensions of the plate and the rigid cone are as follows:

(a) plate: length 3176 mm, width 1588 mm, height 500 mm,
(b) cone: bottom hexagon side 230 mm, top hexagon side 690 mm, height 440 and 300 mm.

The FE model is shown in Fig. 3 and due to symmetry of the problem, only a half of the plate and cone is modelled. The model has 30 216 degrees of freedom, including 5036 nodes and 5511 elements for the plate, and 113 nodes and 96 rigid elements for the cone.

Two types of the boundary conditions were applied at the bottom outer frame of the plate; either three displacements were set to zero, or the vertical displacements and the rigid body motions were restrained. Besides, at the nodes on the plane of symmetry, the symmetry conditions were imposed.

The cone was treated as a perfectly rigid body of mass 80, 160, or 240 tons, and it was constrained to move only vertically.

For the plate, we assumed the elastic-plastic Huber–Mises material of the following parameters: Young's modulus $E = 210$ GPa, Poisson's ratio $v = 0.3$, density $\rho = 7800$ kg/m^3. The plastic material properties, i.e. the yield stress vs. plastic strain curves, are shown in Fig. 4a and b. In Fig. 4a the following curves are shown:

M1. Yield stress $\sigma^Y = 330$ MPa, linear isotropic hardening with ultimate yield stress $\sigma^Y = 450$ MPa at the equivalent plastic strain equal to 1.0.

M2. As M1 + the failure characterised by the stress value equal to zero, a drop in stress value is initiated at the strain 0.3 and reaches zero at 0.35.

M3. Up to the maximum stress the data was taken from the experiment described in [9], Fig. 2 for the bottom plating. Then, a pure plastic flow was assumed.

M4. In the whole range, the data was taken from the experiment described in [9], Fig. 2 for the bottom plating. Note that the complete material failure occurs at strain equal to 0.35.

The constitutive curves, obtained by courtesy of Prof. J. Amdahl from the Faculty of Marine Technology of the Norwegian University of Science and Technology (NTNU), are shown in Fig. 4b,
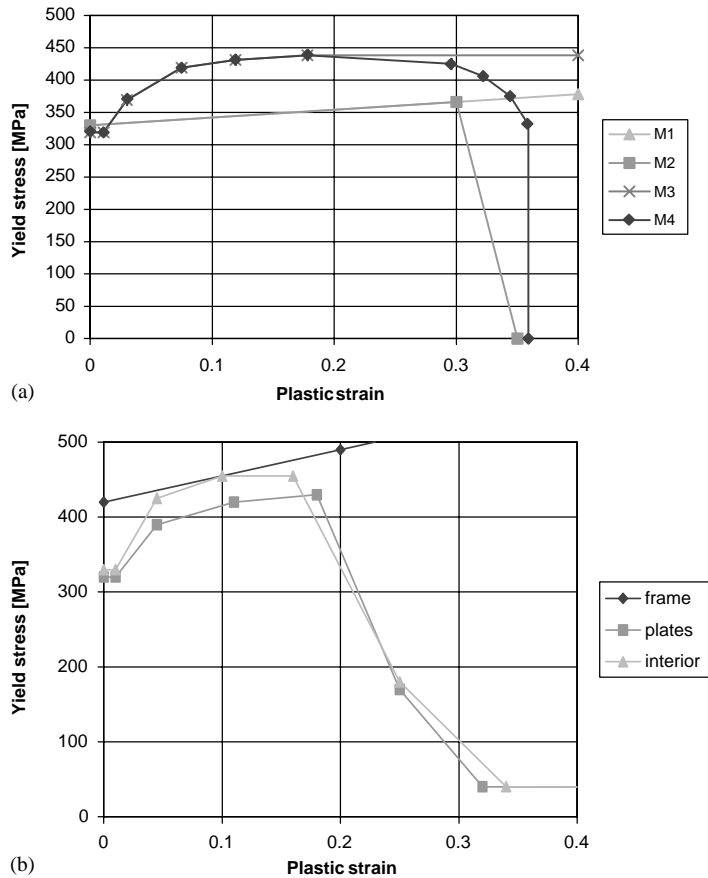
Fig. 4. (a) Constitutive curves adopted in this paper for cone-plate impact; (b) constitutive curves used by Amdahl and Kavlie [9].

and denoted hereafter as M5. These curves are different for different parts of the structure, and the curves for the top/bottom plates and the interior of the plate (i.e. walls, girders and stiffeners) end up by a pure plastic flow at the 10% of the initial yield stress.

The yield stress is defined in the input file as a tabular function of the equivalent plastic strain. The program interpolates the yield stress at a given strain from this table of data; the last defined yield stress is used for the strain greater than the last defined strain value (the curve extends horizontally).

For material models which incorporate the failure of material, the elements exhibiting large plastic strains are removed from the model if the ultimate strain limit is exceeded in all integration (Gauss) points of an element.

Two types of the contact, both without a friction, were tested:

C1: the contact of the outer surface of the cone and a selected node set through the whole plate; these plate nodes are marked by small triangles in Fig. 3.

C2: the contact within interior of the double-hull plate. Initially, 96 contact pairs were defined, but then to overcome difficulties in computations, only the most important 32 contact pairs were
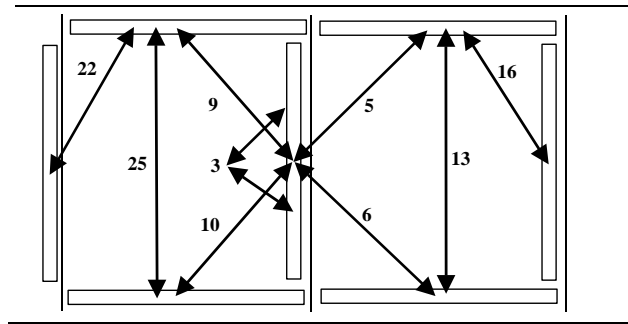
Fig. 5. Contact pairs within plate interior.

selected. In Fig. 5, a cross-section of the plate is schematically shown and the contact pairs are marked by arrows.

In computation, the initial velocity of the cone was 3 m/s, and the time of physical process simulated was up to 0.4 s.

3.3. Numerical analyses and results

The analysed impact/contact process consists of the following stages: (a) the cone is moving with initial velocity given, (b) a contact between the plate and cone is initiated, (c) the plate is deformed and undergoes large rotations and large plastic strains, in which tearing can also appear; a mutual contact and self-contact of the internal plate parts is initiated. (d) the cone is decelerated, and can even be rebounded if its kinetic energy is too small.

Several analyses were performed for the defined FE model, with various combinations of the following parameters:

- material (constitutive) parameters (material curves M1–M5),
- material failure (incorporated into M2 and M4),
- contact definitions (C1, C2),
- mass of the cone (80, 160, or 240 tons).

Below, the selected results of these analyses are presented.

3.4. Influence of selected parameters of analysis

3.4.1. Mass of the striking cone

The effect of the mass of the cone was assessed for combination of M1+C1, i.e. without accounting for material failure and without the internal contact of plate elements. Analyses were performed for cones of mass equal to 80, 160 and 240 tons, and for 240 tons the cone entirely passed through the plate.

The crushing force is the total contact force between the plate and the cone, calculated from the deceleration of the cone on use of the 2nd Newton's law of dynamics $F = ma$. The displacement of the cone describes also the penetration of the plate by the cone, because at the zero time the cone
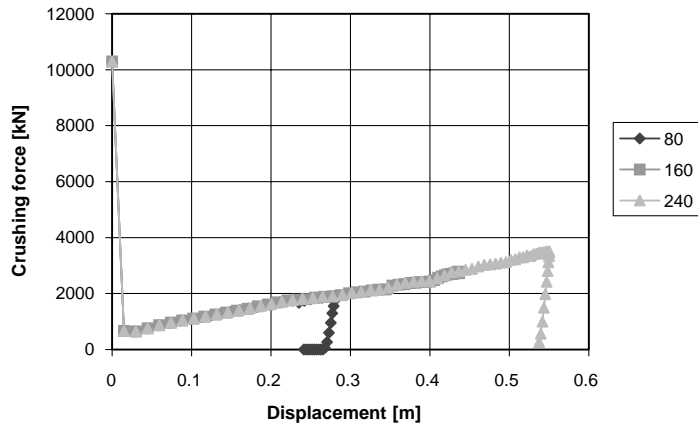
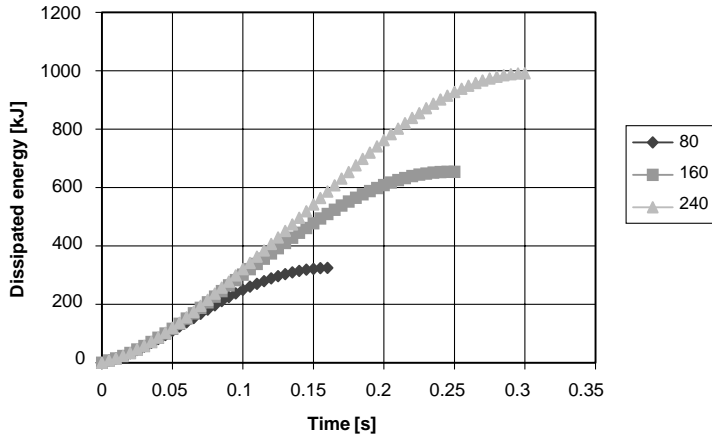Fig. 6. Crushing force vs. displacement of cone (M1).

Fig. 7. Dissipated energy vs. time (M1).

just touches the plate. It can be seen in Fig. 6 that the initial parts of curves for various masses coincide and a curve for a larger mass always extends the curve for a smaller mass. The effect of the rebound (elastic spring-back, with the motion in the reverse direction) is represented by almost vertical branches for 80 and 240 tons.

The amount of energy dissipated at particular time instant and the total dissipated energy depends on the mass of cone. The relation between the dissipated energy and time is shown in Fig. 7.

3.4.2. Material model for the plate

The effect of the material model assumed for the plate on the calculated plate response was assessed for the cone mass of 240 tons and for the contact type C1, with large strains taken into consideration. First we validated the presence of the material softening and failure in the constitutive model. The curves for the material without the failure M3, and for the material including the failure M4 are shown in Fig. 8, and we can see that if the material failure is ignored then the maximum
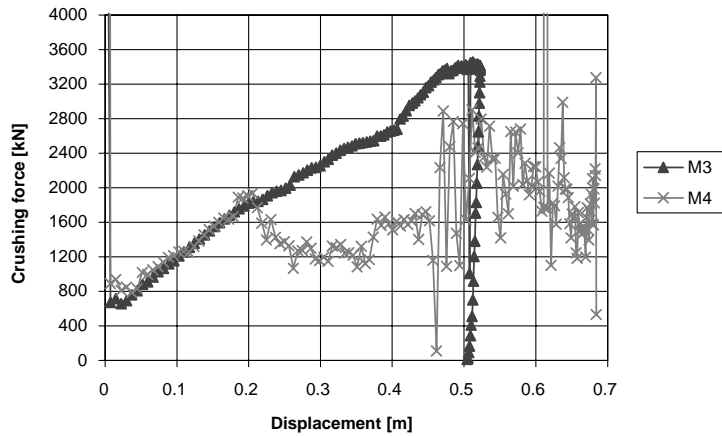
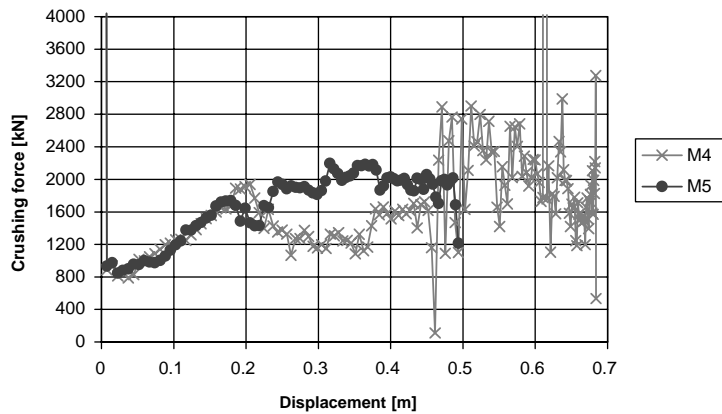Fig. 8. Crushing force vs. displacement for M3 and M4. Cone of mass 240 tons.

Fig. 9. Crushing force vs. displacement for M4 and M5. Cone mass of 240 tons.

crushing force is overestimated. The quasi-oscillatory character of M4 in Fig. 8 is caused not only by a limited number of the sampling points used to create this plot, but also by removal of relatively large finite elements, in which excessive plastic strains occurred.

Besides, the strain at which the material softening is initiated also seems to be important. This effect is shown in Fig. 9 by the results for the material M4, and for the material M5, where the softening starts earlier and a full material failure is not present (some residual bearing capacity is retained). In the calculations for M5 not only the contact C1 is defined, but also the contact C2, within the plate interior. C2 may also be responsible for the increase of the crushing force, after the displacement of 0.3 m has been reached.

A deformation of the plate for the 700 mm cone displacement is shown in Fig. 10. Tearing of the plating is modelled indirectly, by removing the elements with excessive plastic strains from the FE model. For M5, strains are distributed differently and are passed to the bottom plate much earlier.
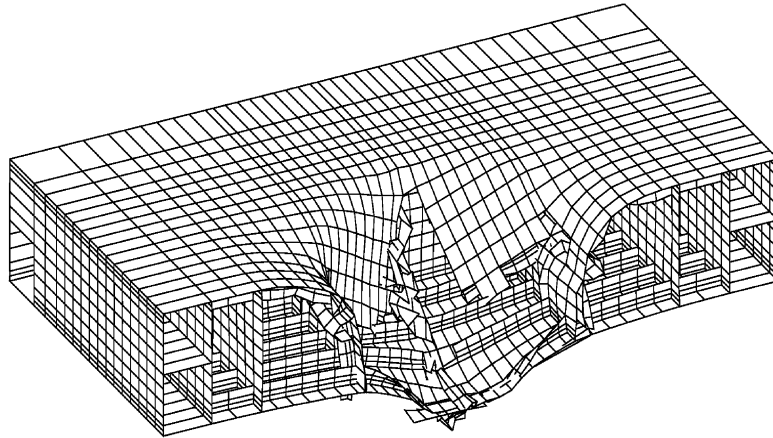
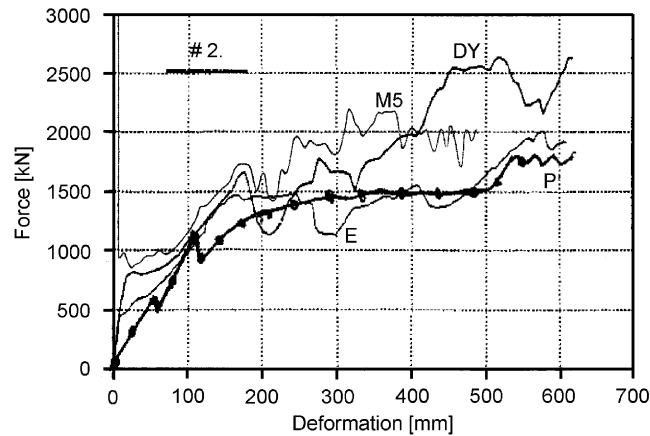Fig. 10. Deformed plate after cone impact.

Fig. 11. Comparison of various results.

The plate elements subjected to C1 exhibit considerable shape distortions, and hence a fine FE mesh is needed to model these deformations accurately.

3.5. Comparison with other results

Comparison with the results obtained elsewhere is shown in Fig. 11. This includes the experimental results [9], curve (E), the results from numerical simulation using the DYNA3D code [9], curve (DY), and the results obtained employing a simplified approach by Simonsen [10], curve (P). The results obtained for model M5 are marked by (M5).

From Fig. 11 we can see that all curves are to certain extent similar, despite differences in computer codes used in calculations and the constitutive curves. A comparison of our numerical results and those of [9] indicates that they are generally in accord. It seems that our computations yielded results, which are closer to the experimental results, as the maximum crushing force of the

experiment does not exceed 2000 kN, and our results for M5 also stay at this level, while those of [9] reach even 2500 kN. Differences in computed results can be attributed to the lack of details regarding computations in [9], especially for the contact definition. Besides, computations in [9] were performed before 1992, when codes were at a different stage of development than today, though even in our computations we had to limit the number of contact surfaces to the most crucial ones.

4. Collision of two ships

4.1. Description of ships participating in collision

The data for ships in collision is by courtesy of Prof. J. J. Jensen from the Department of Naval Architecture and Offshore Engineering of the Technical University of Denmark (DTU). The struck ship is a 105 400 DWT double hull crude oil carrier, for which the main data is as follows: length 234 m, breadth 42 m, depth 21 m, draught 14.9 m, displacement 122 870 t.

The striking ship is a 40 000 DWT container vessel, with the bow consisting of a conventional bow and a bulbous bow. The data for this ship is as follows: length 211.5 m, breadth 32.2 m, depth 24 m, draught 11.9 m, displacement 54 000 t, stem angle $61.5°$. For the bulbous bow we assumed: length 7.5 m, vertical span 10.2 m, horizontal span 5.0 m.

The ships collide at the angle of $90°$. The struck ship is still, while the striking ship is moving. Only a horizontal forward motion of the striking ship is allowed, and its initial velocity in the direction perpendicular to the struck ship is set to 7 knots (3.6 m/s). The crude oil carrier is hit by the container vessel, in the middle between two web frames located near the mid-ship section (see Fig. 12).

The collision is modelled as a pure structure–structure interaction, and the fluid-structure interaction is not taken into account. Hence, we can find the energy dissipated by the friction between both ships and by the plastic deformations, but not by the surrounding water.

4.2. Finite element models of the ships and input data

The striking ship is modelled as a rigid body. The FE model of the bow consists of 148 nodes, and 134 rigid finite elements, of which 124 are 4-noded, and 10 are 3-noded. Note that because the used elements are rigid hence it is not needed to keep the element aspect ratio at about 1.0. The only aim is to provide a good representation of the modelled geometry so consequently the mesh has been made dense in places where the curvatures of the bow are high (e.g. bulbous bow tip) and pretty sparse elsewhere, however maintaining the outer surface of the striking ship smooth enough (no protruding vertices) and convex.

The middle part of the struck ship was selected for the FE modelling, and the geometrical data was read from technical drawings. In a direction perpendicular to the ship axis, approximately a quarter of the deck and a corresponding quarter of the bottom of the ship hull plus the connecting vertical side were modelled. The modelled part of the struck ship consists of eight structural groups: frames, outer hull plating, deck, inner hull plating, outer hull longitudinal stiffeners, longitudinal stiffeners connecting outer and inner hull plating, inner hull longitudinal stiffeners and deck stiffeners. Structural elements are made of two steel types (mild and H.T. steel) and have walls of different thickness values, ranging from 11 to 18.5 mm. The number of the degrees of freedom for the struck ship is
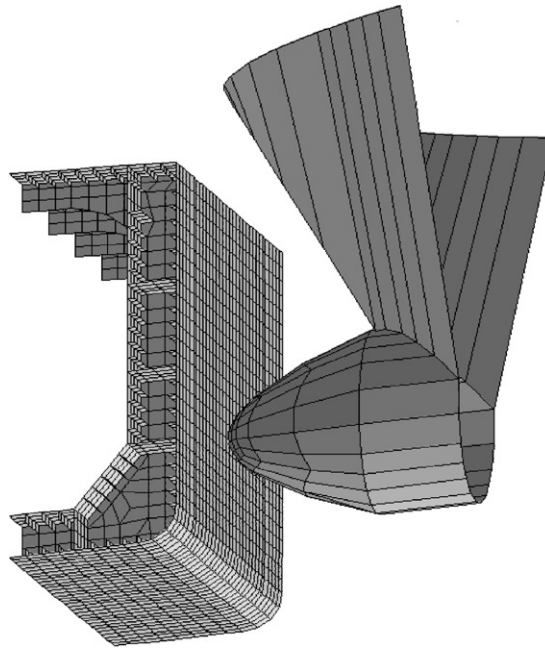
Fig. 12. Relative position of the ships in first instant of impact.

30 792, including 5132 nodes and 5512 shell finite elements, predominantly 4-noded, with 28 of them 3-noded.

For the struck ship, we assumed the elastic–plastic Huber–Mises material of the following parameters: Young's modulus $E = 210$ GPa, Poisson's ratio $v = 0.3$, density $\rho = 7800$ kg/m^3. Two plastic material characteristics were applied:

M1 Steel according to DTU recommendations (elastic-perfectly plastic model):

Satisfies the minimal value of the yield stress specified by the Det Norske Veritas (DNV) Classification Rules, but uses a lower value of the ultimate plastic strain.

Mild steel (*Grade A, B*): Yield stress $\sigma^Y = 235$ MPa, no hardening, ultimate plastic strain equal to 0.1,

H.T. steel (*Grade A*): Yield stress $\sigma^Y = 315$ MPa, no hardening, ultimate plastic strain equal to 0.1.

M2 Steel according to experimental curves (elastic-plastic model with hardening):

The experimental curves for the tension tests were obtained on the closed loop servo-hydraulic universal testing machine MTS810, and are by courtesy of Dr G. Socha of the IFTR PAS, Warsaw. The steel was manufactured by ILVA (Italy) and by RAUTARUUKKI (Finland). From the experimental curves we derived the steel characteristics M2 in such a way that:

- the yield stress σ^Y has the same (minimum) value as specified by DNV Classification Rules,
- the ultimate plastic strain is equal to 0.17, as specified by DNV Classification Rules, and also as obtained in the experiments,
- the shape of the stress–strain curve is similar to the experimental curve.
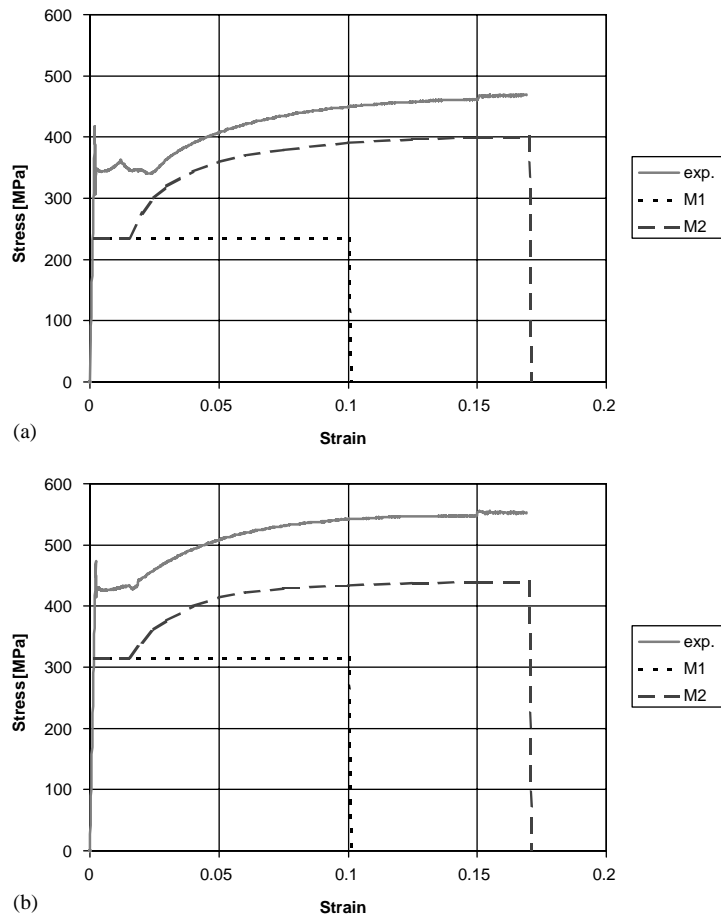
Fig. 13. Constitutive curves for (a) mild steel, (b) H.T. steel.

Mild steel (*Grade A, B*): Yield stress $\sigma^Y = 235$ MPa, tensile strength $R_m = 400$ MPa, ultimate plastic strain equal to 0.17.

H.T. steel (*Grade A*): Yield stress $\sigma^Y = 315$ MPa, tensile strength $R_m = 440$ MPa, ultimate plastic strain equal to 0.17.

Material characteristics, i.e. the stress–strain curves, for M1 and M2 as well as the experimental curves are shown in Fig. 13.

The boundary conditions for the struck ship are applied at four planes: (a) at two vertical bounding planes, the first one in the front and the second one in the rear of the model, (b) at two vertical planes, cutting off the deck and the bottom parts. For nodes belonging to the aforementioned planes all three displacement components were set to zero.

Two following types of contact have been considered:

C1: Contact of the striking bow, treated as a rigid surface, and a set of nodes of the struck ship. This type of contact was included in all analyses. Friction was taken into account, and the following values of the friction coefficient were used: 0.0, 0.1, 0.3 and 0.6.
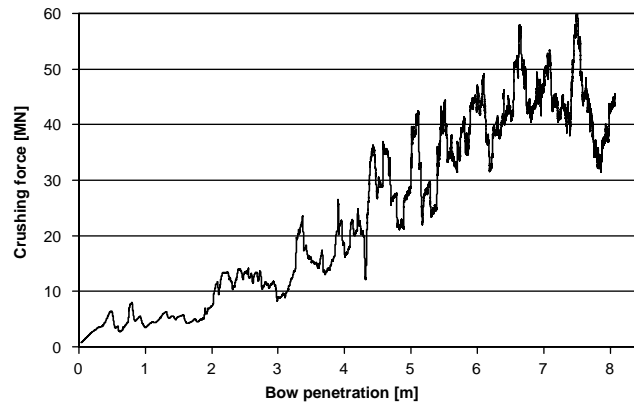
Fig. 14. Crushing force vs. bow penetration for A4.

C2: The contact within the interior of the double-hull of the struck ship. Due to a large distance between the inner and outer plating as well as a relatively small value of the ultimate plastic strain this type of contact was not physically important and hence finally not included.

4.3. Numerical analyses and reference results

Ten analyses were performed for the defined FE models of colliding ships, to establish the influence of various parameters. The reference results provides the analysis A4, which was performed for the material M1, the friction coefficient is equal to 0.6 for contact C1, the displacement boundary conditions, and no mass scaling.

4.3.1. Crushing force vs. bow penetration

The 2nd Newton's law of dynamics, $F = ma$, was utilised to calculate the crushing force from the mass and the decelerations of the striking rigid bow provided by the FE program. The deceleration was monitored for all time steps, the number of which exceeded 150 000; this number was reduced by an automatic selection by the moving average to about 1000 points.

It can be observed in Fig. 14 that the crushing force gradually increases with the penetration, which indicates that the striking bow decelerates at this stage more than at the beginning of the collision. Besides, the curve has many local ups and downs, which may be caused not only by complexity of the deformation process but also by numerical effects such as

- removal of the finite elements in which the ultimate plastic strain is exceeded in all Gauss points, and
- the contact algorithm, which exploits only a set of discrete points for the struck ship.

4.3.2. Energy transformation

From Fig. 15 we can see that a sum of the strain, frictional and kinetic energy remains equal to the initial kinetic energy, which indicates that the numerical algorithm properly conserves the energy.
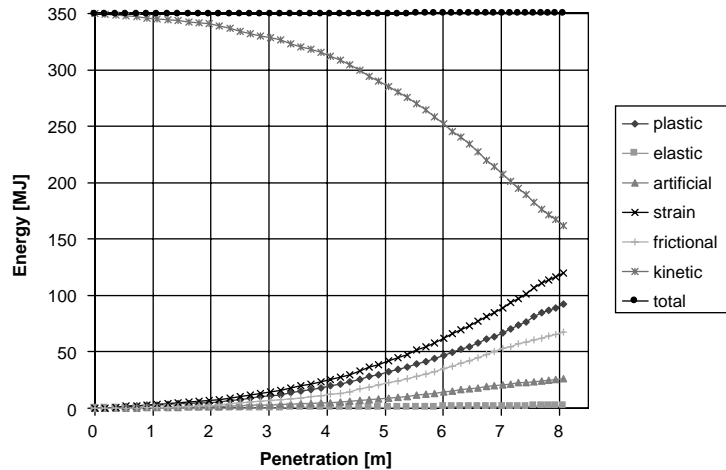
Fig. 15. Energy vs. bow penetration for A4.

The kinetic energy decreases and this is compensated by an increase of the strain and frictional energies.

The strain energy consists of the following parts: the plastic energy, which is the highest one, the elastic energy, which is negligible, and the "artificial" energy associated with stabilisation of singular modes of the FE model.

The energy curves are smooth because they are produced by using the displacement and velocity only, unlike the crushing force, which is based on the deceleration.

4.3.3. Struck ship deformation

Fig. 16 depicts the struck ship final deformation. All the elements, for which the ultimate plastic strain was exceeded in all Gauss points, were removed from the plots. It can be noticed that, after the element removal, the hole in the struck ship closely resembles the geometry of the rigid bulbous bow. Also the deck indentation is similar to the shape of the upper part of the striking bow.

In these figures some of the elements are not connected to the main part, i.e. are "flying", which is the result of a removal of their adjacent elements where an excessive plastic strain occurred. Such "flying" parts are a normal phenomenon in the explicit codes, and are used e.g. to model the trajectories of disrupted parts after a blast.

4.4. Influence of selected parameters of analysis

Comparisons of results of analyses A1–A10 allow us to evaluate influence of selected parameters, such as mass scaling, boundary conditions, friction coefficient, material characteristics, additional velocity component and initial velocity of the striking ship.

4.4.1. Mass scaling

The so-called mass scaling is a numerical technique designed to speed up computations. The smallest (or stiffest) elements in the FE mesh always drastically limit the length of the time step
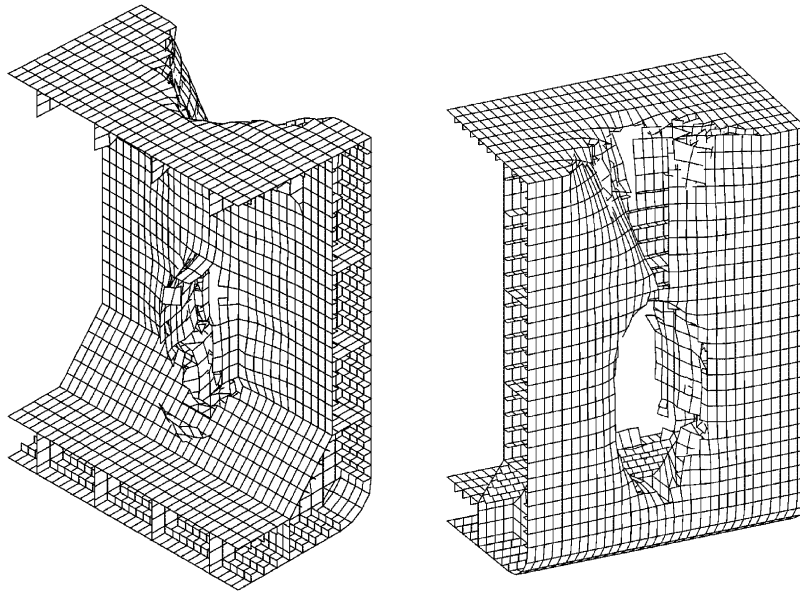
Fig. 16. Damage of the struck ship after impact for A4.

applied. By increasing the mass of such elements the time step is tailored to middle-sized elements and computations are faster. The larger the mass scaling factor, the higher the speed up ratio obtained. However, this technique is acceptable only when its influence on results is minor. This technique was applied with the mass scaling factor equal to 100, which gives the speed up ratio equal to 10. Next, for comparison, the analysis without the mass scaling was carried out. It turned out that the mass scaling significantly affects the kinetic, strain and plastic energy as well as the crushing force. To avoid difficulties in interpretation of results, this technique was not used in further analyses.

4.4.2. Boundary conditions

Two types of the boundary conditions were applied at the nodes along the struck ship model edges in the front, rear, bottom and deck part: either all displacements or all displacements and rotations were suppressed. The obtained results indicate that the crushing force is insensitive to the boundary condition types checked. A similar conclusion is true for the energies. Hence, only the boundary displacements were suppressed in further analyses.

4.4.3. Friction coefficient

It is difficult to assess the actual value of the friction coefficient, therefore a parametric study for the values equal 0.0, 0.1, 0.3 and 0.6 was performed. To separate the effect of the friction coefficient, the same values of the other parameters were used.

Fig. 17 shows that the higher the friction coefficient, the faster the loss of kinetic energy observed. This result is in accord with the engineering intuition, which says that the friction speeds up the process of energy dissipation in any impact/contact process. We can also see that the difference between the curves for 0.3 and 0.6 is much smaller than between the curves for 0.0 and 0.3, hence,
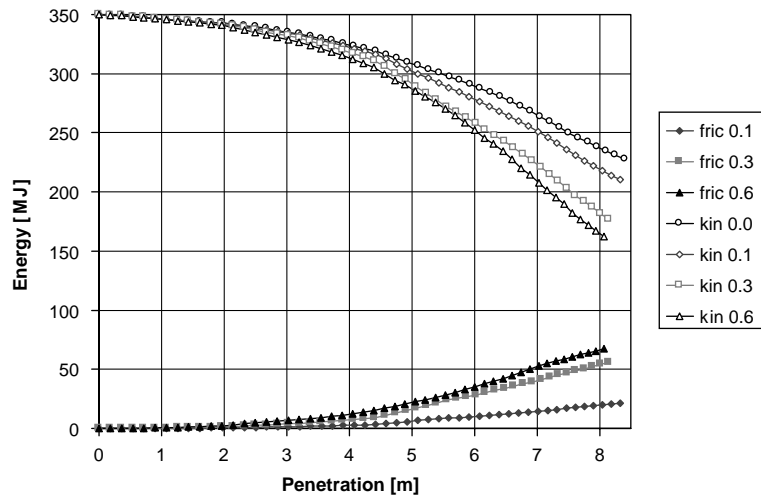
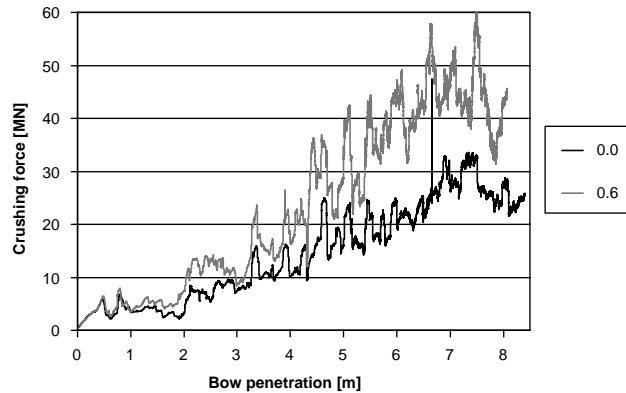Fig. 17. Influence of friction coefficient on kinetic and frictional energies.

Fig. 18. Influence of friction coefficient on crushing force.

we can expect that the effect of the friction will not become remarkable for values of the coefficient larger than 0.6 (rarely used in engineering practice).

In Fig. 18 we can see that, in comparison to the case with no friction, the crushing force significantly increases when the friction coefficient equal to 0.6 is applied.

4.4.4. Constitutive relations

The results for two constitutive models M1 and M2, and the friction coefficient equal to 0.6, are compared in Figs. 19 and 20.

Fig. 19 shows that the plastic energy dissipated in the collision is much higher for M2 than for M1, and e.g. for the 7 m penetration, it is two times higher. Looking at Fig. 20 we see that the crushing force is also significantly greater for M2 than for M1. This fact can be translated into a quicker deceleration of the striking ship. Also the kinetic energy for M2 is decreasing quicker with
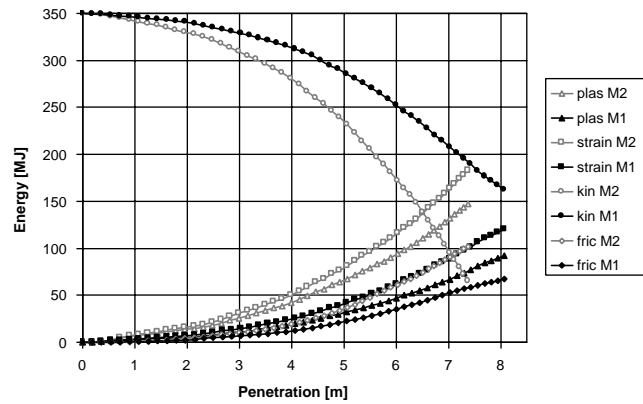
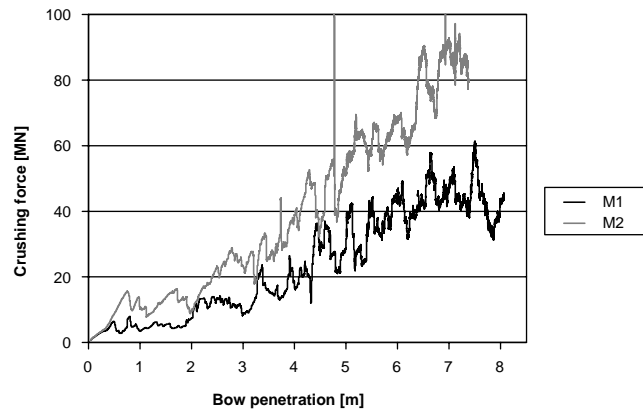Fig. 19. Energies for M1 and M2.

Fig. 20. Crushing force for M1 and M2.

the penetration, as shown in Fig. 19. We can conclude that M1 is quite conservative in comparison with the experiment-based M2. As current FE codes admit constitutive curves of a complicated form, it seems rather reasonable to use the experimental curves similar to M2 in FE calculations, and control safety via a separate factor.

We can observe similar tendencies for the case with no friction, though the kinetic energy decreases faster in the presence of friction.

4.4.5. Additional velocity in Y direction of the striking ship

The Y-direction is parallel to the longitudinal axis of the struck ship and is perpendicular to the striking ship motion used in other analyses. The striking ship has a velocity of 7 knots in X-direction, and 3.5 knots in Y-direction. The Y-component of the velocity was introduced in order to evaluate the effect of the struck ship motion in the simplest possible way. The simplification in this analysis consists in assigning the Y-component of velocity to the striking ship, instead of the struck ship. Note that it is not indifferent, which ship this additional velocity is assigned to, because the struck ship has 2.5 times bigger mass.
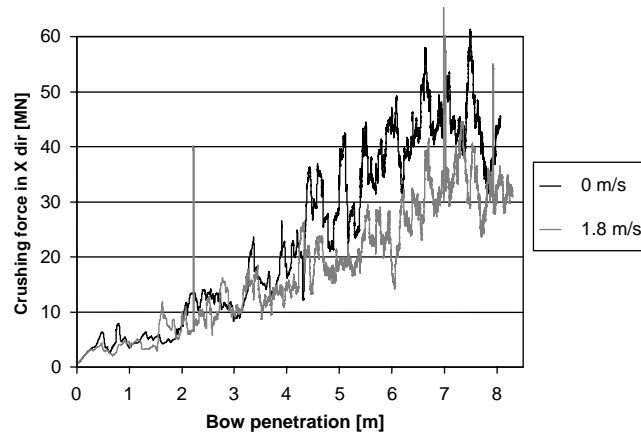
Fig. 21. Influence of velocity in Y-direction on crushing force in X-direction.
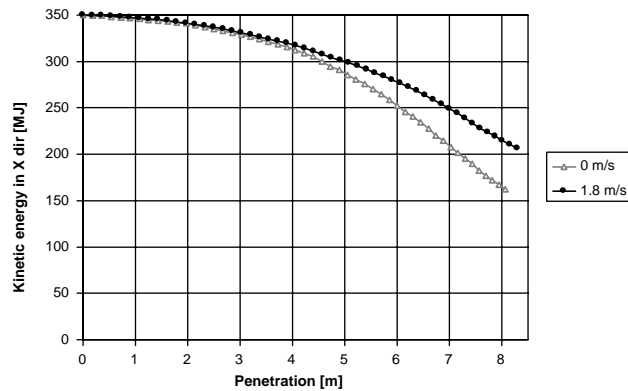

Fig. 22. Influence of velocity in Y-direction on kinetic energy in X-direction.

The orientation of the striking bow remains unchanged, and it is normal to the longitudinal axis of the struck ship throughout the whole analysis.

The results of the analysis with the additional velocity in Y-direction and the analysis without it are compared in Figs. 21 and 22. The X-component of the crushing force, depicted in Fig. 21 is generally smaller for the analysis with the additional velocity component. Consequently, the deceleration is slower, and the loss of kinetic energy shown in Fig. 22 is also slower. This is likely to be due to the fact that the contact between both ships is now maintained only at one side of the striking bow, while a widening gap occurs at the other side. Hence, we can expect that the depth of penetration will be greater for the case with the additional velocity component. This also indicates that the case when the struck ship is not moving and remains still is not the worst case in terms of the expected damage.
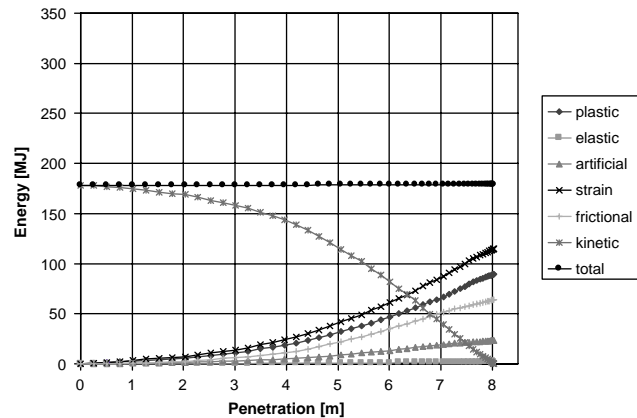
Fig. 23. Energies for initial velocity equal 5 knots.

4.4.6. Initial velocity

The initial velocity in the reference analysis A4 was 7 knots (3.6 m/s), and the analysis was carried out until about the 8-m indentation of the struck ship was obtained, i.e. for about 2.5 s.

For comparison, the initial velocity of the striking ship was reduced from 7 to 5 knots (2.57 m/s), which reduced the initial kinetic energy almost two times, from 350 to 178 MJ. Besides, the process was slower in time and the analysis was run longer for 5 s after the impact. Hence, at the end of analysis, the final velocity was equal to zero, while in the reference analysis A4 it was about 2.5 m/s. In this way, we captured the moment when the whole kinetic energy was dissipated by the plastic deformation and friction, for the friction coefficient equal to 0.6.

It is interesting to see in Fig. 23 that, from the moment when half of the kinetic energy is dissipated, i.e. for the 6-m penetration, the kinetic energy curve almost linearly decreases to zero. It reaches zero at the 8-m penetration, i.e. when in A4 only half of the energy is dissipated. Assuming a similar character of the kinetic energy curve for A4, one can predict that then the maximum penetration, at which the striking ship stops, should be about 11 m.

The dynamics of the collision was different in both analyses, but comparing the crushing force vs. penetration curves, only small differences between these curves were identified, which indicates that the deceleration/penetration ratio is similar. Also the energy dissipated in these analyses, shown as functions of the penetration, are almost the same. This confirms that by relating the different dynamic processes to the penetration we can compare them in a meaningful way.

5. Final remarks

The obtained results have been discussed in detail in the previous sections while here some additional comments are made, having in mind future simulations of ship collisions.

5.1. Numerical method

- Using the explicit method implies intrinsic dependence of the time integration scheme upon the mesh size applied. Elimination of damaged finite elements in the material tearing process locally

reduces the mass of the structure and may cause oscillations to structural response and produce extremely high instantaneous values (cf. crushing force in Figs. 8, 9, 14, 18, 20, 21). A local divergence in the explicit time integration may occur in spite of the permanent control of time step, which is always tailored to the smallest (stiffest) element in the FE mesh.

5.2. Striking ship velocity and relative motion of the vessels

- In our computer simulations, the striking bow was treated as rigid, which was very convenient, because the number of degrees of freedom of a rigid bow was reduced to 6. Nonetheless, its geometry was almost exactly represented, which rendered that the contact between the ships and the damage of the struck ship was quite realistically modelled.
- Our results indicate a need for an exact initial velocity data for the striking ship, because it has a great influence on the extent of damage of the struck ship, as the kinetic energy depends on velocity square.
- It was shown that both velocity components are important, not only the normal to the direction of the struck ship centre line. The tangent velocity (roughly modelling the struck ship motion) changes significantly the collision process, as then the contact between both ships is maintained only at one side of the striking bow. As a consequence, the kinetic energy is dissipated slower, so we can expect a bigger hole and a deeper penetration.

5.3. Material model for the struck ship

- Our results show that large deformations and plastic strains dominate in the struck ship, while the elastic energy in negligible. Hence, constitutive modelling of the plastic part is essential, therefore two models were compared: the simple M1, suggested by the DTU, and the experiment-based DNV-compliant model M2. The conclusion is that M1 is quite conservative in comparison with M2 e.g. the plastic energy is two times smaller for M1, which is equivalent to application of the safety factor equal to 2.
- Current FE codes admit complicated constitutive curves, which can be specified as piece-wise linear functions. Hence, in FE computations we can use the experimental curves, similar to M2, and control safety via a separate factor.
- Peaks of the deceleration and the crushing force curves are due to two features of the FE model: (a) the finite elements with the excessive plastic strains are removed from the model, which is essential for modelling of tearing; (b) the contact is defined for a finite set of nodes of the struck ship. In both cases, a finer mesh and smaller elements may reduce these peaks, but the analysis will certainly be more CPU time-consuming.

Finally, we note that though a dynamic FE code is used, the crushing force and the dissipated energy are presented as functions of the rigid bow penetration and hence our plots can be compared with results of a static analysis, for which the bow displacement is an independent parameter.

Acknowledgements

References

[1] V.U. Minorsky, An analysis of ship collisions with reference to protection of nuclear power ships, J. Ship Res. 3 (2) (1959) 1–4.

[2] P.T. Pedersen, S. Zhang, Absorbed energy in collision and grounding—revising Minorski's Empirical method, J. Ship Res. 44 (2) (2000) 140–154.

[3] H. Lenselink, K.G. Thung, Numerical simulations of the Dutch–Japanese full scale ship collisions tests, The MacNeal-Schwendler Company Report, Gouda, The Netherlands, 1992.

[4] T. Wierzbicki, Crushing behaviour of plate intersections, in: N. Jones, T. Wierzbicki (Eds.), Structural Crashworthiness, Butterworth & Co. Publishers Ltd, London, 1983. (Chapter 3)

[5] T. Wierzbicki, Concertina tearing of metal plates, Int. J. Solids Struct. 32 (19) (1995) 2923–2943.

[6] A. Sano, O. Muragishi, T. Yoshikawa, T. Motoi, A. Murakami, Strength analysis of a new double hull structure for VLCC in collision, Proceedings of the International Conference on Designs and Methodologies for Collision and Grounding Protection of Ships, San Francisco, August 1996, paper 8-1.

[7] B.C. Simonsen, H. Ocackli, Experiments and theory on deck and girder crushing, Thin-walled Struct. 34 (1999) 195–216.

[8] K. Wisniewski, P. Kolakowski, B. Rozmarynowski, J.T. Gierlinski, Dynamic FE simulation of damage in ships collision, Proceedings of ICCGS 2001 (Second International Conference on Collision and Grounding of Ships), Copenhagen, Denmark, July 1–3, 2001.

[9] J. Amdahl, D. Kavlie, Experimental and numerical simulation of double hull stranding, DNV-MIT Workshop on Mechanics of Ship Collision and Grounding, DNV Høvik, Oslo, September 1992.

[10] B.C. Simonsen, Basic modelling principles and validation of software for prediction of collision damage, ISESO Report no. I108.02.02.052.004, Department of Naval Architecture and Offshore Engineering, Technical University of Denmark, April 2000.

[11] O. Kitamura, FEM approach to the simulation of collision and grounding damage, Proceedings of the ICCGS 2001 (Second International Conference on Collision and Grounding of Ships), Copenhagen, Denmark, July 1–3, 2001.